Spin gap and dynamics in $Sr_{14-x}Ca_xCu_{24}O_{41}$ comprising hole-doped two-leg spin ladders: Cu NMR study on single crystals

K. Magishi
Department of Physical Science, Graduate School of Engineering Science, Osaka University, Toyonaka, Osaka 560, Japan and CREST, Japan Science and Technology Corporation (JST), Japan

S. Matsumoto, Y. Kitaoka, K. Ishida, and K. Asayama
Department of Physical Science, Graduate School of Engineering Science, Osaka University, Toyonaka, Osaka 560, Japan

M. Uehara, T. Nagata, and J. Akimitsu
Department of Physics, Aoyama-Gakuin University, Chitosedai, Setagaya-ku, Tokyo 157, Japan
(Received 2 May 1997; revised manuscript received 31 December 1997)

We report comprehensive Cu NMR studies on single crystals of $Sr_{14-x}Ca_xCu_{24}O_{41}$, which contain simple CuO_2 chains and two-leg Cu_2O_3 ladders. From measurements of the ^{63}Cu NMR shift, it is clear that the spin gap in the ladders decreases with isovalent Ca substitution from $\Delta=550\pm30$ K for $Sr_{14}Cu_{24}O_{41}$ (Sr14) to 350 ± 30 K, 280 ± 30 K, and 270 ± 30 K for $x=6$ (Ca6), $x=9$ (Ca9), and $x=11.5$ (Ca11.5), respectively. The exponential decrease of the nuclear spin-lattice relaxation rate $1/T_1$ below ~130 K is consistent with the presence of the spin gap in the spin excitation spectrum. In the T range higher than ~200 K, we observed the following dependences: $1/T_1=$const and the square of Gaussian spin-echo decay time, $T_{2G}^2 \propto T$ which are consistent with the scaling theory for the $S=1/2$ one-dimensional (1D) Heisenberg model. The value of $T_{2G}/T_1\sqrt{T}$ is compatible with the theoretical prediction of an exchange constant along the leg $J_{\parallel}\sim1800$ K for Ca6 and $J_{\parallel}\sim1500$ K for Ca9 and Ca11.5. A notable finding is that the magnitude of the spin gap remains nearly constant and characteristics of novel 1D-like spin dynamics are maintained in the content varying from Ca9 to Ca11.5. On the other hand, the charge transport changes with increasing Ca content so that the more conductive Ca11.5 exhibits pressure-induced superconductivity exceeding 3.5 GPa. We have found that T_{2G}^2, which is proportional to the inverse spin correlation length ξ^{-1}, deviates from a linear T dependence upon cooling and is described by $A+BT\exp(-\Delta/T)$, regardless of the Ca substitution. We point out that the value of $T_{2G}^2(T=0)=A$ is proportional to the finite value of $\xi_0^{-1}=\Delta/c_{1D}$, where $c_{1D}=(\pi/2)J_{\parallel}$ is the spin-wave velocity. From the result that the values of $A^{-1}\sim\xi_{\rm eff}$ for Ca6, Ca9, and Ca11.5 are significantly reduced compared to that for Sr14, it is suggested that $\xi_{\rm eff}$ is dominated at low T by an average distance d among mobile holes obeying the relation $\xi_{\rm eff}\sim d=\xi_h$. From an estimate of $\xi_0/a\sim5.2$ for Sr14, where a is the Cu-Cu distance along the leg, ξ_h/a is obtained as ~3.5, 2.3, and 2.0, and hole content x as ~0.14, 0.22, and 0.25 per Cu_2O_3 ladder for Ca6, Ca9, and Ca11.5, respectively. These values were consistent with $x=0.14$, 0.2, and 0.22 for Ca6, Ca9, and Ca11 estimated from the optical conductivity experiment by Osafune *et al.* [Phys. Rev. Lett. **78**, 1980 (1997)]. The $Sr_{14-x}Ca_xCu_{24}O_{41}$ compounds are thus hole-doped two-leg spin-ladder systems which reveal the metallic behavior dominated by the 1D-like spin dynamics at high T and accompanied by the spin gap formation at low T. For Ca11.5, as the spin gap is formed upon cooling below ~180 K, the resistivity increases in the direction perpendicular to the ladder, whereas the conductivity along the ladder remains metallic, followed by the localization of mobile holes in both directions below $T_L\sim60$ K. We point out that preformed pairs are confined in each ladder and localized below ~60 K at an ambient pressure. [S0163-1829(98)02718-0]

I. INTRODUCTION

Recently, Uehara *et al.* have discovered superconductivity with $T_c=12$ K under a pressure of 3 GPa in $Sr_{0.4}Ca_{13.6}Cu_{24}O_{41.84}$.[1] Superconductivity was confirmed in the single crystal of $Sr_{2.5}Ca_{11.5}Cu_{24}O_{41}$ by an application of pressure greater than 3.5 GPa.[2] All high-T_c cuprate superconductors found up to now contain two-dimensional (2D) square CuO_2 planes, whereas this new cuprate superconductor is comprised of the two-leg Cu_2O_3 ladders and the CuO_2 chains. From extensive studies on the quasi-one-dimensional (1D) $S=1/2$ two-leg spin-ladder systems,[3] the presence of the spin gap was theoretically predicted[4,5] and subsequently established from susceptibility, NMR, and neutron scattering experiments on $(VO)_2P_2O_7$ (Refs. 6,7) and $SrCu_2O_3$.[8,9] In this context, it is important that the parent material for the cuprate superconductor is a Mott insulator with a spin gap in contrast to the antiferromagnetic (AF) insulator in the case of high-T_c cuprates.

$(La,Sr,Ca)_{14}Cu_{24}O_{41}$ into which holes are doped was initially reported by MaCarron *et al.*[10] and Siegrist *et al.*[11] This compound with an orthorhombic symmetry is comprised of the 1D-CuO_2 chains, the (Sr,Ca) layers, and the two-leg Cu_2O_3 ladders as illustrated in Fig. 1. Each layer is alternately stacked along the b axis with spacing of ~3.2 Å, which is shortened by the Ca substitution. The susceptibility

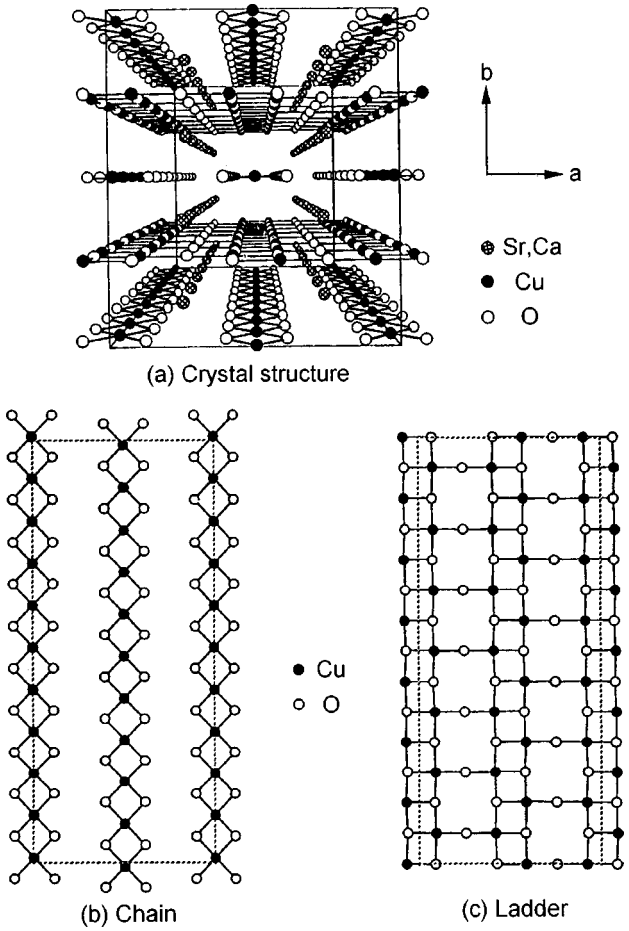

FIG. 1. (a) The crystal structure of $(Sr,Ca)_{14}Cu_{24}O_{41}$. (b) and (c) show the CuO_2 chain and Cu_2O_3 ladder subunit, respectively.

and ESR measurements revealed the presence of spin gap in the chains with $\Delta_{chain}=120-133$ K,[12–15] whereas the NMR T_1 on $Sr_{14}Cu_{24}O_{41}$ (denoted as Sr14)[16,17] and the inelastic neutron scattering experiments on the $(Sr_{0.8}Ca_{0.2})_{14}Cu_{24}O_{41}$ (Ref. 18) showed the presence of spin gap with $\Delta_{ladder}\sim 700$ and ~ 400 K in the ladders, respectively. A significant aspect of this ladder material is that the nominal Cu valence is $+2.25$, i.e., holes are inherently doped and the conductivity increases upon isovalent Ca substitution. However, it was suggested that the holes only enter the structural unit of the CuO_2 chains that have an average $Cu^{+2.6}$ valence.[12,15] It was suggested that the residual moments formed the singlet-triplet gap from the dimerization as a result of the nonmagnetic CuO_2 unit breaking up the chains.

Recently, Matsuda *et al.* showed from the inelastic neutron experiment that the dimers are formed between spins which are separated by 2 and 4 times the distance between the nearest-neighbor copper ions in the chain sites.[19] From this result, the alternate array of Cu^{2+} and Cu^{3+} along the chains was suggested with an average valence of $Cu^{+2.5}$ and $Cu^{+2.07}$ for the chains and the ladders, respectively. Recent NMR studies have resolved three Cu valence states in the chain sites, e.g., magnetic Cu^{2+} sites forming the dimerized state and two Cu^{3+}-like sites.[20,21] A recent x-ray measurement has revealed that the periodic lattice distortion develops in the chains below 200 K.[22] From the result that the nuclear relaxation process, measured by NQR at the ladder Cu sites, is caused by fluctuations of the electric field gradient (EFG), slow motion of doped holes and/or lattice distortion have also been suggested.[21]

The substitution of Ca in the Sr sites increases the conductivity of $Sr_{14-x}Ca_xCu_{24}O_{41}$,[12,13,15] although the average Cu valence does not change due to the isovalence of the Ca substitution. Three possible scenarios for the hole distribution have been proposed. Namely, (1) most of holes are on oxygen atoms in the chains.[15] (2) Holes in the ladders become conductive in addition to a transfer of holes from the chains to the ladders.[23] (3) For the undoped compound, most of holes are on the chains, whereas upon the Ca substitution for the Sr sites, holes are transferred from the chains to the ladders.[12,24,25] Recently, the third scenario was supported by the calculation of the electronic state.[26] From measurements of the nuclear spin-lattice relaxation rate $1/T_1$ on polycrystal samples, a spin gap existing in the ladders was reported to decrease linearly up to the $x=9$ compound, whereas the spin gap in the chains hardly changes.[17] The T_1 measurement for the single crystal showed that the spin gap decreased from 830 ± 30 K for $Sr_{14}Cu_{24}O_{41}$ to 350 ± 30 K for the $x=11.5$ compound.[23,27] Its magnitude was larger than that extracted from the average T_1 data on the polycrystal samples. Note that T_1 in the single crystals was precisely measured with a single component, whereas T_1 in the polycrystal samples was not reliable since a Gaussian distribution of T_1 was assumed. Furthermore, we have reported a preliminary result that the spin correlation length ξ_h in the Ca-doped systems is dominated by a mean distance among mobile holes, and the hole content x is tentatively estimated to be $x=0.25$ for Ca11.5 using the relation $\xi_h=(2x)^{-1}$.[27]

In this paper, we present the comprehensive results for the T dependences of the NMR shift and T_1 of ^{63}Cu in the ladder sites on single crystals of $Sr_{14}Cu_{24}O_{41}$ and Ca-doped $Sr_{14-x}Ca_xCu_{24}O_{41}$ with $x=6$ (hereafter denoted as Ca6), $x=9$ (Ca9), and $x=11.5$ (Ca11.5). Comprehensive Cu NMR/NQR measurements of the single crystals of $Sr_{14}Cu_{24}O_{41}$ have been recently reported for both the chains and the ladders by Takigawa *et al.*[21] In our experiments, we report different NMR results in the ladder Cu sites on single crystal of $Sr_{14}Cu_{24}O_{41}$ regarding the size in spin gap and the characteristics in spin dynamics. Furthermore, we have obtained the following notable results for hole-doped two-leg spin-ladder systems.

(1) A spin gap in the ladder Cu sites for Sr14 is significantly reduced upon isovalent Ca substitution, but its magnitude saturates with $\Delta=280\pm 30$ K and 270 ± 30 K for Ca9 and Ca11.5, respectively.

(2) From the result that the spin correlation length is dominated by an average distance among mobile holes in Ca6, Ca9, and Ca11.5, an effective hole density is estimated to be ~ 0.14, 0.22, and ~ 0.25 per Cu_2O_3 ladder for Ca6, Ca9, and Ca11.5, respectively.

(3) Even though holes are doped into the two-leg spin-ladders and the resistivity follows a T-linear dependence along the ladders, the spin dynamics at high temperatures is characterized for $T\geqslant\Delta$ by a behavior similar to that of the $S=1/2$ 1D Heisenberg systems.

(4) The spin-gap formation in the metallic state between 60 and 130 K causes an anisotropic resistivity through an

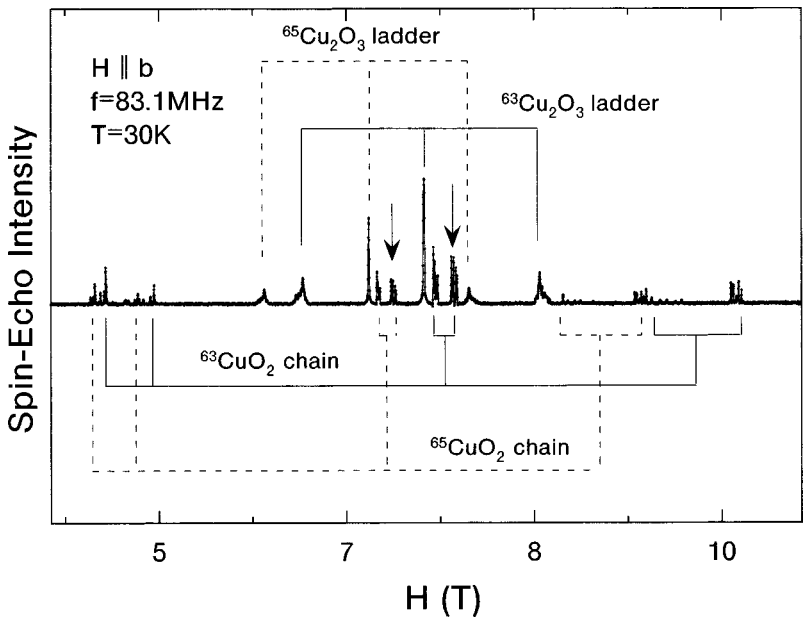

FIG. 2. The Cu NMR spectrum in $Sr_{14}Cu_{24}O_{41}$ at $T=30$ K obtained by sweeping the magnetic field along the b axis at $f=83.1$ MHz.

increase in resistivity in the perpendicular direction to the ladders.

(5) A confinement of preformed pairs is indicative of a precursor effect for the occurrence of the pressure-induced superconductivity in Ca11.5.

II. EXPERIMENTAL PROCEDURES

Single crystals were grown by the traveling-solvent floating-zone method. Detailed procedures for synthesizing single crystals were reported elsewhere.[2] Their single crystallinity was confirmed by the x-ray Laue method. The susceptibilities of Ca6, Ca9, and Ca11.5 indicate a plateau around 80 K followed by a Curie-like upturn at low T. Measurements of the ^{63}Cu NMR shift were made in a T range of $4.2-300$ K with a frequency range of $81.1-125.1$ MHz. An NMR spectrum was obtained by a sweeping magnetic field generated by a superconducting magnet (12 T at 4.2 K). The nuclear spin-lattice relaxation time T_1 was measured by the saturation recovery method with a single T_1 component except at temperatures lower than ~ 100 K. The nuclear relaxation function $R(t)$ for the central transition $(1/2 \leftrightarrow -1/2)$ for $I=3/2$ among the quadrupole split lines is given by[28]

$$R(t)=\frac{M(\infty)-M(t)}{M(\infty)}=0.9\ \exp\left(-\frac{6t}{T_1}\right)+0.1\ \exp\left(-\frac{t}{T_1}\right), \tag{1}$$

where $M(t)$ is the nuclear magnetization at time t after the saturation pulses. The spin-echo amplitude E recorded as a function of time τ between the first and second pulses was well fitted to the expression[29]

$$E(2\tau)=E_0\ \exp\left[-\left(\frac{2\tau}{T_{2L}}\right)-\frac{1}{2}\left(\frac{2\tau}{T_{2G}}\right)^2\right], \tag{2}$$

where $1/T_{2G}$ is the Gaussian spin-echo decay rate associated with the indirect nuclear spin-spin coupling through electronic excitations and $1/T_{2L}$ is the Lorentzian decay rate associated with the T_1 process. $1/T_{2L}$ was determined from the expression $1/T_{2L}=3(1/T_1)_{\parallel}+(1/T_1)_{\perp}$ (Ref. 30) where $\parallel$ and $\perp$ indicate the b axis and a or c axis, respectively.

III. EXPERIMENTAL RESULTS AND DISCUSSIONS

A. $Sr_{14}Cu_{24}O_{41}$

1. ^{63}Cu NMR spectrum

Figure 2 shows the NMR spectrum for Sr14 with a magnetic field (H) along the b axis at $T=30$ K and $f=83.1$ MHz. The spectrum consists of many sharp peaks, which originate from the ladder and chain Cu sites with different nuclear quadrupole tensors ν_b along the b axis for two ^{63}Cu and ^{65}Cu isotopes.

A site assignment for each NMR peak is denoted in the figure. The ^{63}Cu site with $\nu_b=13.4$ MHz is assigned to the ladder Cu site, since the $\nu_{b,\max}$ of its maximum component of the electric field gradient tensor is close to $\nu_{c,\max}=10.15$ MHz in the ladder Cu site in $SrCu_2O_3$.[9] The Cu site with $\nu_b=32.9$ MHz is hence assigned to the chain Cu site because the spin gap of $120-133$ K was actually observed as previously reported.[12–15]

There are two sets of NMR spectra exhibiting the same T dependence for each isotope in the chains. The NMR peaks indicated by thick arrows pointing downwards arise from the chain Cu sites, which are included in the twine of the single crystals. The multipeak structure observed in the NMR spectra of the chain Cu sites is associated with a long period for the superstructure.[21,22] At temperatures below 30 K, another signal appears. Its shift shows a stronger T dependence than those of other signals, suggesting that it originates from the magnetic Cu^{2+} sites forming the dimerized state with a gap of 120 K.[20] These NMR results for the chain Cu sites are consistent with those reported by Takigawa *et al.*[21]

2. Knight shift

In general, the Knight shift $K(T)$ in copper oxides consists of the T independent orbital part $K_{\rm orb}$ and the T-dependent spin part $K_s(T)$:

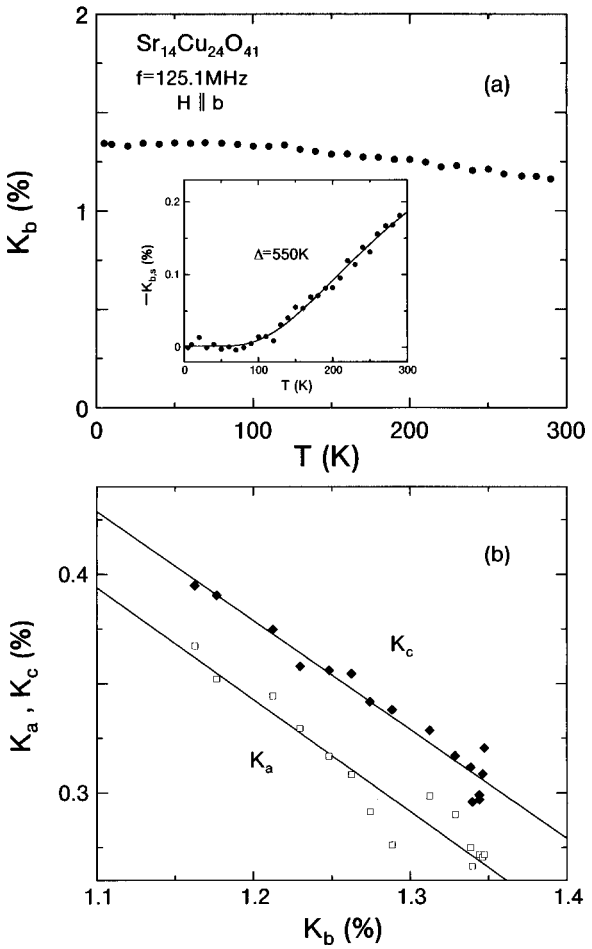

FIG. 3. (a) T dependence of the ^{63}Cu Knight shift in $Sr_{14}Cu_{24}O_{41}$ for $H\| b$ axis. The inset displays the T dependence of the spin part in ^{63}Cu Knight shift $K_{s,b}(T)$. Solid line is a fit to $T^{-1/2}\exp(-\Delta/T)$ with $\Delta=550$ K. (b) displays $K_b(T)$ vs $K_a(T)$ ($\diamond$) and $K_b(T)$ vs $K_c(T)$ ($\blacklozenge$) plots.

$$K_\alpha(T)=K_{\mathrm{orb},\alpha}+K_{s,\alpha}(T) \quad (\alpha=a,b, \text{ and } c),$$

$$K_{\mathrm{orb},\alpha}=2\langle 1/r^3\rangle\chi_{\mathrm{orb},\alpha},$$

$$K_{s,\alpha}=A_\alpha(q=0)\chi_{s,\alpha}/N_A\mu_B,$$

where χ_{orb} and χ_s are the van Vleck and spin susceptibilities, respectively. $A_\alpha(q)=\Sigma_j A^j_\alpha \exp(iqr_j)$.

For the spin-ladder systems with the spin gap Δ the expression for the spin susceptibility $\chi_s(T)$ was derived in the low-temperature regime by Troyer *et al.*[31] as

$$\chi_s(T)=\frac{C}{\sqrt{T}}\exp(-\Delta/T).$$

Figure 3(a) indicates the T dependence of $^{63}K_b$ for Sr14. The residual Knight shift approaches 1.32% at $T=4.2$ K. This value is comparable to that in high-T_c cuprates, so the observed residual Knight shift is attributed to the orbital contribution. From the relations of $K_{s,b}(T)=K_b(T)-K_{\mathrm{orb},b}=[A_b(0)/N_A\mu_B]\chi_s(T)$ with $K_{\mathrm{orb},b}=1.32\pm0.01\%$, the spin part $K_{s,b}(T)$ in the NMR shift is obtained. The spin Knight shift is dominated by the inner core polarization effect of $3d$ electrons and its sign is negative. Figure 3(b) shows K_a vs K_b and K_c vs K_b plots with temperature as the implicit parameter. From the respective slopes, $A_b(0)/A_a(0)=A_b(0)/A_c(0)=-2$ are obtained. By using $K_{\mathrm{orb},b}=1.32\%$, $K_{\mathrm{orb},a}=0.28\%$ and $K_{\mathrm{orb},c}=0.32\%$ are estimated.

$K_{s,b}(T)$ is displayed in the inset of Fig. 3(a). A best fit to the above formula allows us to estimate the energy gap to be $\Delta_K=550\pm30$ K, which is somewhat larger than $\Delta_K=420\pm20$ K estimated by Takigawa *et al.*[21] An uncertainty in the gap value in the present measurement arises from the uncertainty in $K_{\mathrm{orb},b}$.

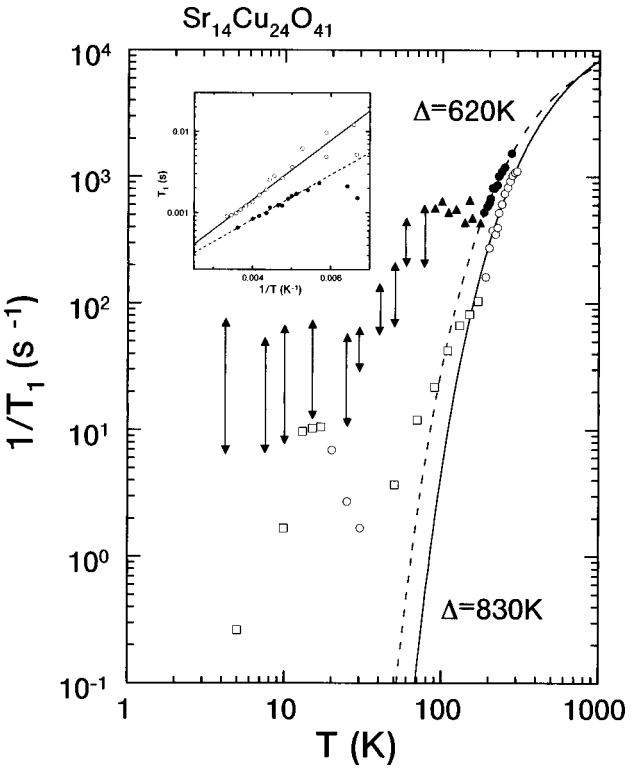

FIG. 4. T dependences of $^{63}(1/T_1)$ in both logarithmic scales in $Sr_{14}Cu_{24}O_{41}$ for $H\| b$ axis ($\bigcirc$) and at zero field by NQR ($\bullet$). Solid lines are fits to $1/T_1\sim\exp(-\Delta/T)$ with $\Delta=830$ K for $H\| b$ and 620 K for NQR, respectively. Inset is T_1 vs $1/T$ plot in semilogarithmic scale.

3. Nuclear spin-lattice relaxation rate $1/T_1$

Figure 4 indicates the T dependences of $^{63}(1/T_1)$ for $H\| b$ ($\bigcirc$,$\square$) at 11 T by NMR and at zero field by NQR ($\bullet$,$\blacktriangle$,$\blacktriangledown$). As seen in the figure, $1/T_1$ depends on the external magnetic field.

The nuclear relaxation in the 1D spin-chain and spin-ladder systems with the spin gap occurs dominantly via the two-magnon Raman process, in which a thermally excited magnon $|k,\sigma\rangle$ is scattered into the state $|k+q,\sigma'\rangle$ by the hyperfine interaction, accompanied by nuclear spin flop. Since magnons are excited only around $k_x\simeq\pi$ along the chain as required by the energy conservation law, the main contribution to $1/T_1$ comes from the region $q\sim0$ in spite of strong short-range AF spin correlations around $q=\pi$. In such a case, due to the diffusive spin dynamics near $q\sim0$, $1/T_1$ was shown to follow the field dependence of $1/\sqrt{H}$.[32,33] Taking account of only these processes, Troyer *et al.* obtained the leading low-temperature form[31]

$$1/T_1 \sim |A(0)|^2 \exp(-\Delta_{T_1}/T). \quad (3)$$

In the case of NQR, since the relaxation function of the nuclear magnetization $R(t)=[M(\infty)-M(t)]/M(\infty)$ is a simple exponential relation in the T range higher than 200 K, $1/T_1$ is uniquely determined and is well fitted by the form of $1/T_1 \propto \exp(-\Delta/T)$ with $\Delta=620$ K as shown by the dotted line. On the other hand, $R(t)$ below ~ 200 K changes into a multiexponential behavior. In order to see an overall T dependence of $1/T_1$ below ~ 200 K, we plotted tentative values of $1/T_1$ as estimated from the short ($\triangle$) and the long ($\triangledown$) decays in the $R(t)$ curve. Down to 80 K, only the short component is reliably deduced. The bar for the data below 200 K does not indicate an error but a range in the distribution of $1/T_1$. Around 200 K, $1/T_1$ for NQR deviates from an activated behavior associated with periodic lattice distortions in chains. It was reported that the nuclear relaxation in the T range of $30-150$ K was dominantly caused by fluctuations of the local electric field gradient via the nuclear quadrupole coupling $(1/T_1)_Q$ showing a peak near 100 K.[21] When the inverse correlation time $(1/\tau_c)$ of EFG fluctuations is equivalent to the NQR frequency $(\omega_{\rm NQR})$, i.e., $1/\tau_c=\omega_{\rm NQR}$, $(1/T_1)_Q$ becomes largest.[21] Therefore, it has been proposed that a probable source of the EFG fluctuations is the motion of the holes in the ladders.

In the case of NMR, $1/T_1$ is uniquely determined with a single component above ~ 200 K from the relaxation function of Eq. (1). $1/T_1$ in a T range above 200 K is fitted to $\exp(-\Delta_{T_1}/T)$ with $\Delta_{T_1}=830\pm 30$ K. A deviation from the activation law is seen below 200 K as in the case of NQR. The relaxation function is not fitted by the form of Eq. (1) with a single T_1 component. This is because the relaxation process is affected by the quadrupole relaxation.[21] In contrast to the case of NQR, $1/T_1$ measured at 125.1 MHz does not exhibit any maximum around 100 K. The quadrupole relaxation rate $(1/T_1)_Q$ becomes largest when $1/\tau_c=\omega_{\rm NMR}$ $(10^{10}\ {\rm s}^{-1})$. It is expected that the temperature at which $(1/T_1)_Q$ peaks increases from 100 K to a temperature higher than 200 K. This is because $1/\tau_c$ is reported to increase upon heating from $10^8\ {\rm s}^{-1}$ at 100 K to $10^9\ {\rm s}^{-1}$ at 200 K.[21] In such a high temperature region, since the relaxation process is dominated by magnetic fluctuations, it is anticipated that a peak of $(1/T_1)_Q$ associated with the quadrupole relaxation process will not be observed in the NMR experiment.

Notably, we have again found that the relaxation process is dominated by magnetic relaxation below 30 K and that $1/T_1$ has a peak around 20 K. Takigawa *et al.* reported that a peak in the magnetic relaxation rate $(1/T_1)_M$ is observed around 10 K and it is presumably due to the spin fluctuations of magnetic impurities.[21] Alternately, we propose another scenario to explain a peak in $1/T_1$ around 20 K. As the motion of the holes slows upon cooling, it is likely that a singlet coherence in the spin-gap state is disturbed and hence spin fluctuations may be induced. When the frequency of spin fluctuations approaches the NMR frequency (125.1 MHz) around 20 K, $1/T_1$ may have a peak. As presented later, this is the case in the Ca-doped compounds in which mobile holes start to localize below $T_L \sim 60$ K, where $1/T_{2L}$ peaks.

In most of the spin gap systems including Sr14, the spin gap Δ_{T_1} deduced from the activation law of $1/T_1$ is $1.4-1.8$ times larger than Δ_χ from the susceptibility and the NMR shift.[9,33–36] Several scenarios to explain this discrepancy have been proposed theoretically.

(1) There will be large contributions to $1/T_1$ from processes with $q_x \sim \pi$ and $q_y=\pi$ between the one-magnon branch at $k_x \simeq \pi$ and the continuum at $k_x \sim 0$ if the temperature where T_1 is actually measured is high enough for the states at energies exceeding the gap to be populated.[37] This is because the ladder has strong short-range AF correlations.

(2) Based on the Majorana fermion representation of the $S=1/2$ Heisenberg two-leg spin-ladder systems, Kishine and Fukuyama found that the spin susceptibility and the NMR-T_1 have different activation energies with $\Delta_{T_1}=\sqrt{3}\Delta_\chi$ in the high-T range, but $\Delta_{T_1}=\Delta_\chi$ in the low-T range, which is consistent with our experiment.[38]

(3) Based on the 1D-gapped quantum nonlinear σ model, Sachdev and Damle developed an effective classical model for spin transport at low T and obtained the value of the spin diffusion constant.[39] As a result, they derived

$$\frac{1}{T_1} \propto |A(0)|^2 \sqrt{\frac{T}{H}} \exp(-3\Delta/2T),$$

$$\chi \propto \sqrt{\frac{\Delta}{T}} \exp(-\Delta/T).$$

In the above equations, note that the activation gaps for Δ_χ and Δ_{T_1} satisfy $\Delta_{T_1}=1.5\Delta_\chi$, even at low T. In any case, a quantitative comparison of each scenario with experiments requires a detailed study of the H and T dependences of $1/T_1$.

B. Ca-doped $Sr_{14-x}Ca_xCu_{24}O_{41}$

1. ^{63}Cu NMR spectra and nuclear quadrupole parameters

Figures 5(a), 5(b), and 5(c) display the ^{63}Cu NMR spectra for Ca11.5 with the magnetic field (H) along the b, a, and c axes at $T=4.2$ K and $f=81.1$ MHz, respectively. These spectra originate from the Cu sites in the ladders and chains with different sets of nuclear quadrupole tensors ν_α where $\alpha=a,b$, and c. From a comparison of obtained values with those in Sr14, the ^{63}Cu sites with $\nu_a=-4.2$, $\nu_b=+15.7$, and $\nu_c=-11.5$ MHz were assigned to the ladders with the maximum component of the electric field gradient tensor along the b axis, whereas that with $\nu_a=-15.6$, $\nu_b=+32.6$, and $\nu_c=-17.0$ MHz were assigned to the chain Cu sites.

Figure 6 indicates the NMR spectrum for the central transition $(1/2 \leftrightarrow -1/2)$ for $H \| b$ at $T=150$ K and $f=125.1$ MHz. The intense NMR spectrum arises from the ladder Cu sites, whereas three weak peaks are assigned to different chain Cu sites. This is because the T dependences of the NMR shifts and T_1 are consistent with the presence of a spin gap with $\Delta_{\rm chain}=120-133$ K in the chains. Further details about the magnetic and electronic properties for the chain Cu sites will be reported elsewhere.[20]

The position of the central transition $(1/2 \leftrightarrow -1/2)$ for the ladder is affected by the Knight shift and the second-order quadrupole shift in each direction. In this case, the shift of the resonance field $(\omega-\gamma_N H_{{\rm res},\alpha})/\gamma_N H_{{\rm res},\alpha}$ is expressed by the Knight shift K_α and the EFG component ν_α in terms of the second-order perturbation theory as follows:[40,41]

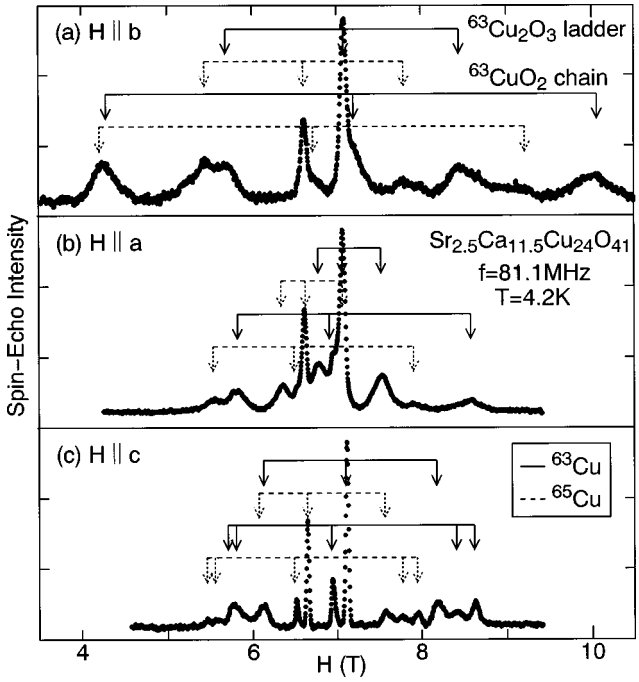

FIG. 5. The Cu NMR spectra at $T=4.2$ K and $f=81.1$ MHz for (a) $H\| b$ axis, (b) $H\| a$ axis, and (c) $H\| c$ axis in $Sr_{2.5}Ca_{11.5}Cu_{24}O_{41}$.

$$\frac{\omega-\gamma_N H_{\mathrm{res},\alpha}}{\gamma_N H_{\mathrm{res},\alpha}}=K_\alpha+\frac{(\nu_\beta-\nu_\gamma)^2}{12(1+K_\alpha)(\gamma_N H_{\mathrm{res},\alpha})^2},$$

where $(\alpha,\beta,\gamma)=(a,b,c)$ and the magnetic field $H_{\mathrm{res},\alpha}$ is the resonance field along each crystal axis, γ_N is the nuclear gyromagnetic ratio of ^{63}Cu, and ω is the NMR frequency. In order to separate the Knight shift from the quadrupole shift, the frequency (magnetic field) dependence of the spectrum has been measured at several different frequencies in the range of 81.1−125.1 MHz as seen in Fig. 7. From the respective slopes of $(\omega-\gamma_N H_{\mathrm{res},\alpha})/\gamma_N H_{\mathrm{res},\alpha}$ vs $(\gamma_N H_{\mathrm{res},\alpha})^{-2}$ plots, ν_a, ν_b, and ν_c are estimated to be -4.3, $+15.6$, and -11.6 MHz, which are consistent with those obtained from the spacing between adjacent lines in the field-swept spectra in Fig. 2. Each component of the Knight shift K_α is obtained from the intersection at $(\gamma_N H_{\mathrm{res},\alpha})^{-2}=0$.

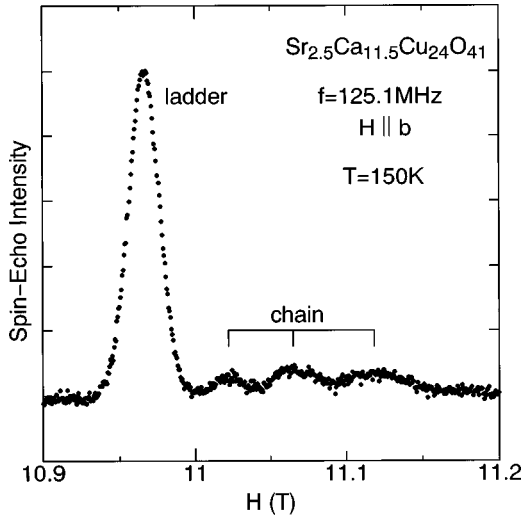

FIG. 6. The ^{63}Cu NMR spectra of the central $(1/2\leftrightarrow -1/2)$ transition for $H\| b$ axis at $T=150$ K and $f=125.1$ MHz in $Sr_{2.5}Ca_{11.5}Cu_{24}O_{41}$. An intense peak originating from the ladder ^{63}Cu sites is well separated from the three peaks from the chain ^{63}Cu sites.

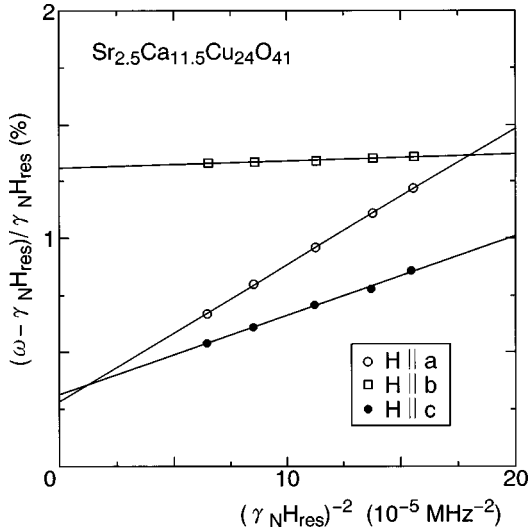

FIG. 7. The $(\omega-\gamma_N H_{\mathrm{res}})/\gamma_N H_{\mathrm{res}}$ vs $(\gamma_N H_{\mathrm{res}})^{-2}$ plots in Ca11.5 in the frequency range of 81.1−125.1 MHz for $H\| a$ axis (○), $H\| b$ axis (□), and $H\| c$ axis (●). From the slope and the intersection at $(\gamma_N H_{\mathrm{res}})^{-2}=0$ of each line, the respective component of the nuclear quadrupole tensor and the Knight shift is obtained, respectively.

2. Knight shift

Figure 8 indicates the T dependences of K_a (○), K_b (□), and K_c (●) of ^{63}Cu for Ca11.5. The respective residual Knight shifts K_b, K_a, and K_c approach 1.32, 0.28, and 0.32 % at $T=4.2$ K, which agrees with the corresponding values in Sr14. According to the Mila-Rice's hyperfine Hamiltonian in high-T_c cuprates,[42] the hyperfine form factor for ^{63}Cu in the CuO_2 plane is expressed as

$$A_\alpha(q)=A_\alpha+2B(\cos q_x a+\cos q_y a),$$

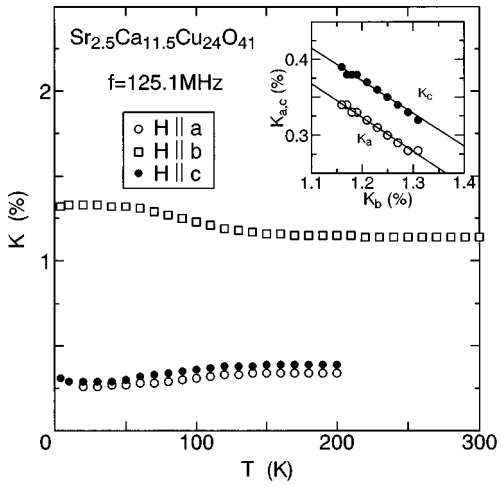

FIG. 8. T dependences of the ^{63}Cu Knight shifts in Ca11.5 for $H\| a$ axis (○), $H\| b$ axis (□), and $H\| c$ axis (●). Inset displays $K_b(T)$ vs $K_a(T)$ (○) and $K_b(T)$ vs $K_c(T)$ (●) plots.

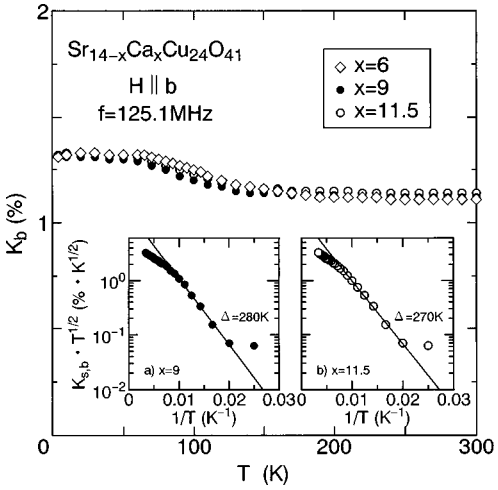

FIG. 9. T dependences of the ^{63}Cu Knight shifts $K_b(T)$ for $H\|$ b axis in Ca6 ($\diamond$), Ca9 ($\bullet$), and Ca11.5 ($\circ$) at $f=125.1$ MHz. The inset is $K_{s,b}T^{1/2}$ vs $1/T$ plot in Ca9 ($\bullet$) and Ca11.5 ($\circ$). $K_{s,b}=K_b-K_{\mathrm{orb},b}$ (=1.32 %). The solid line is the respective fit to $\exp(-\Delta_K/T)$ with $\Delta_K=280$ K and 270 K in Ca9 and Ca11.5.

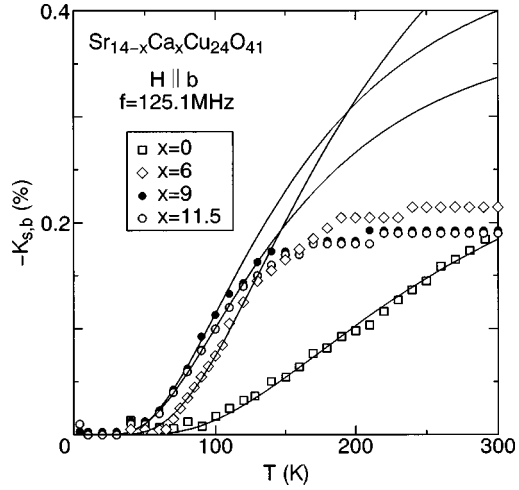

FIG. 10. T dependences of the spin part in ^{63}Cu Knight shifts $K_{s,b}(T)$ for $H\|$ b axis in Sr14 ($\square$), Ca6 ($\diamond$), Ca9 ($\bullet$), and Ca11.5 ($\circ$) at $f=125.1$ MHz. The solid line is a fit to $T^{-1/2}\exp(-\Delta/T)$.

where A_α is the on-site hyperfine field, B is the supertransferred hyperfine field, and a is the Cu-Cu distance.

In optimum and underdoped high-T_c cuprates[43] and linear spin-chain Sr_2CuO_3,[44] $A_c=-164$ kOe/μ_B, $A_{ab}=34$ kOe/μ_B, and $B=41$ kOe/μ_B were estimated from $A_c(0)\sim 0$ and $A_{ab}(0)=196$ kOe/μ_B. In contrast, the hyperfine form factor for the Cu_2O_3 ladder is expressed as follows:

$$A_\alpha(q)=A_\alpha+2B_\alpha\cos q_x a+B_\alpha\cos q_y a \qquad (\alpha=a,b,\text{ and } c).$$

$A_c(0)=A_c+3B_c=-120$ kOe/μ_B and $A_{ab}(0)=A_{ab}+3B_{ab}=48$ kOe/μ_B were obtained from the K vs χ plot for the oriented polycrystal of $SrCu_2O_3$.[9] In Ca11.5, the measured susceptibility is, however, dominated by the chain contribution, so A_α is not determined from the K vs χ plot. Here, note that each layer in $SrCu_2O_3$ is stacked along the c axis, whereas the stacking is along the b axis in the present compound. As indicated in the inset of Fig. 5, from the slope of the plots of $K_b(T)$ vs $K_a(T)$ and $K_c(T)$ with

$$K_b(T)=\frac{A_b(0)}{A_\alpha(0)}[K_\alpha(T)-K_{\mathrm{orb},\alpha}]+K_{\mathrm{orb},b} \quad (\alpha=a \text{ and } c),$$

$A_b(0)/A_c(0)\simeq A_b(0)/A_a(0)\simeq -2.5$ are obtained and $A_c(0)\simeq A_a(0)$. If $K_{\mathrm{orb},b}$ is taken as 1.32% at $T=4.2$ K, $K_{\mathrm{orb},a}$ and $K_{\mathrm{orb},c}$ are estimated as 0.28 and 0.32 %, respectively. These anisotropic orbital shifts in Sr14 and Ca11.5 are comparable to $K_{\mathrm{orb},c}=1.28\%$ and $K_{\mathrm{orb},ab}=0.24\%$ in high-T_c cuprates. It should be noted that $|A_b(0)/A_c(0)|=|A_b(0)/A_a(0)|\simeq 2.5$ in Ca11.5 is equivalent to $|A_c(0)/A_{ab}(0)|=12$ T/4.8 T$=2.5$ in $SrCu_2O_3$,[9] but is larger than $|A_b(0)/A_c(0)|=|A_b(0)/A_a(0)|\simeq 2.0$ in Sr14. It is anticipated that the hyperfine field is dominated by the on-site contribution from the ladder Cu sites.

Figure 9 indicates the T dependences of $K_b(T)$ for Ca6, Ca9, and Ca11.5. The orbital Knight shifts are similar for all compounds. $K_{s,b}\sqrt{T}$ is plotted against $1/T$ in the inset of Fig. 9. A linear best fit allows us to estimate the respective energy gaps to be $\Delta_K=280\pm 30$ K and 270 ± 30 K for Ca9 and Ca11.5. An uncertainty in the gap value arises from the uncertainty in $K_{\mathrm{orb},b}$.

Figure 10 reveals that the spin gap decreases from $\Delta=550\pm 30$ K for Sr14 to 350 ± 30 K, 280 ± 30 K, and 270 ± 30 K for Ca6, Ca9, and Ca11.5, respectively, and that its magnitude is nearly unchanged with the increasing Ca content.

3. Nuclear spin-lattice relaxation rate $1/T_1$

In contrast to the case of Sr14, the relaxation is magnetic in the entire T range for the Ca-doped compounds. For Ca6, Ca9, and Ca11.5, $^{63}(1/T_1)$ is uniquely determined with a single component above ~ 100 K from the relaxation function of Eq. (1) as indicated in the inset of Fig. 11. $1/T_1$'s for all compounds begin to decrease below ~ 200 K. $1/T_1$ are

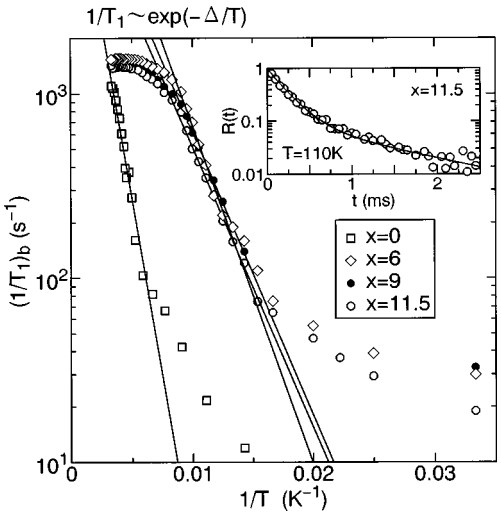

FIG. 11. $(1/T_1)_b$ for $H\|$ b axis vs $1/T$ plots in Sr14 ($\square$), Ca6 ($\diamond$), Ca9 ($\bullet$), and Ca11.5 ($\circ$). The respective solid line is a fit to $1/T_1\sim\exp(-\Delta/T)$ with $\Delta=830$, 450, 360, and 350 K for Sr14, Ca6, Ca9, and Ca11.5. The inset indicates the relaxation function of the nuclear magnetization $R(t)$ at $T=110$ K in Ca11.5.

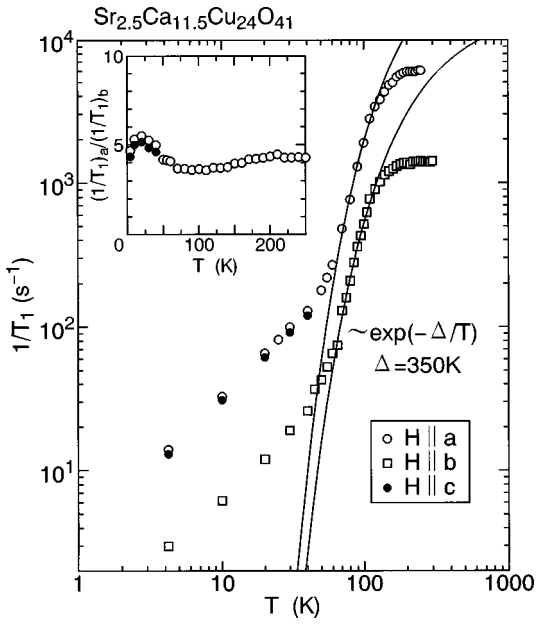

FIG. 12. T dependences of $^{63}(1/T_1)$ in both logarithmic scales in Ca11.5 for $H\|$ a axis (○), $H\|$ b axis (□), and $H\|$ c axis (●). The solid line is a fit to $1/T_1 \sim \exp(-\Delta/T)$ with $\Delta = 350$ K. The inset is the T dependence of the anisotropy, $R=(1/T_1)_a/(1/T_1)_b$.

plotted in Fig. 11 as a function of $1/T$ on a semilogarithmic scale along with the NMR-T_1 data for Sr14 shown in Fig. 4. $1/T_1$ in a T range of 60−130 K is fitted to $\exp(-\Delta_{T_1}/T)$ with $\Delta_{T_1}=450 \pm 30$ K, 360 ± 30 K, and 350 ± 30 K for Ca6, Ca9, and Ca11.5, respectively, which is smaller than $\Delta_{T_1}=830 \pm 30$ K for Sr14. The deviation from the activation law becomes significant for Sr14 at temperatures lower than ~200 K, below which the periodic lattice distortion takes place in the chains.[22] In contrast, $1/T_1$ in Ca6, Ca9, and Ca11.5 deviates from the activation law below ~60 K, where the steep increase in resistivity suggests a localization of mobile holes.[2,45] It should be noted that even in the Ca-doped systems, the size of the spin gap deduced from the NMR-T_1 shift is larger than that determined from the NMR shift.

In order to gain further insights into the relaxation process, we notice three T domains (i) $T \leqslant T_L \sim 60$ K below which mobile holes are localized, (ii) 60 K$\leqslant T \leqslant$130 K, and (iii) 200 K$\leqslant T$ exist. We focus on the anisotropy of the relaxation rate $R=(1/T_1)_a/(1/T_1)_b$. Figure 12 indicates the T dependences of $1/T_1$ for $H\|a$ (○), $H\|b$ (□), and $H\|c$ (●) axes. As indicated in the inset of Fig. 11, $R_{\rm ex}$ in T domains (i) and (iii) is $\sim 5 \pm 1$ and 4.3, respectively, whereas $R_{\rm ex}$ ~3.7 in T domain (ii) is smaller than those in T domains (i) and (iii). Since the relaxation process for $T \ll \Delta$ is dominated by a one-magnon branch around $k_x \sim \pi$, we have a relation

$$R=\frac{(1/T_1)_a}{(1/T_1)_b}=\frac{|A_c(0)|^2+|A_b(0)|^2}{|A_c(0)|^2+|A_a(0)|^2}=\frac{1}{2}\left[1+\left(\frac{|A_b(0)|}{|A_a(0)|}\right)^2\right],$$

noting that $A_a(0) \simeq A_c(0)$. With $|A_b(0)|/|A_a(0)|=2.5$ from the anisotropy of the Knight shift measurement $R_{\rm cal}$ is obtained as 3.6, which is in excellent agreement with the experimental value of $R_{\rm ex}=3.7$ in T domain (ii). This agreement means that $1/T_1$ decreasing exponentially in T domain (ii) is dominated by one-magnon excitations over the spin gap around $k_x \sim \pi$. In T domain (iii) where $\Delta \leqslant T$, $1/T_1$ stays constant, and is dominated by short-range AF correlations at $q_x \sim \pi$, $q_y=\pi$. In this case, R changes from $R_{q\sim 0}$ to

$$R_{q\sim\pi}=\frac{1}{2}\left[1+\left(\frac{|A_b(\pi)|}{|A_a(\pi)|}\right)^2\right].$$

Therefore, an increase of $R_{\rm ex}$ from 3.7 to 4.3 above ~200 K is ascribed to a possible change in the hyperfine form factor. By combining

$$\frac{A_b+3B_b}{A_a+3B_a}=\frac{A_b+3B_b}{A_c+3B_c}=-2.5$$

with the relation

$$\frac{1}{2}\left[1+\left(\frac{|A_b(\pi)|}{|A_a(\pi)|}\right)^2\right]=\frac{1}{2}\left(1+\frac{(A_b-3B_b)^2}{(A_a-3B_a)^2}\right)=4.3,$$

we find that $B_a \simeq B_b \simeq B_c$ and is as small as ~0.6 kOe/$\mu_{\rm B}$. Thus, it is experimentally established that the hyperfine field in the ladder Cu nuclei is dominated by the on-site hyperfine field.

In T domain (i) where $1/T_1$ deviates from the activation behavior, $R_{\rm ex} \sim 5 \pm 1$ is close to ~4.3 as expected for the relaxation process around $q \sim \pi$ in the high T range of T domain (iii). This means that the relaxation process below $T_L \sim 60$ K is dominated by staggered spin fluctuations.

4. Gaussian spin-echo decay rate $1/T_{2G}$

The Gaussian spin-echo decay rate in copper oxides is dominated by indirect nuclear spin-spin coupling through electronic excitations.[29] $1/T_{2G}$ is generally derived as[46,47]

$$\left(\frac{1}{T_{2G}}\right)^2=\frac{p\gamma_N^4\hbar^2}{8\mu_{\rm B}^4}\left(\sum_q A_z(\pi)^4\chi(q)^2-\left[\sum_q A_z^2(\pi)\chi(q)\right]^2\right),$$

where $\chi(q)={\rm Re}\chi(q,0)$ is the static susceptibility. The z axis is in the direction of the external field (b axis) and p is the abundance of the ^{63}Cu isotope. In $SrCu_2O_3$, $1/T_{2G}$ was reported to exhibit a weak T dependence followed by saturation at low T.[9] The calculation of $1/T_{2G}$ based on the quantum Monte Carlo technique by Sandvik *et al.* was in good agreement with the experimental result with an isotropic exchange constant $J_\parallel=J_\perp=850$ K, where $J_\parallel$ and $J_\perp$ are the AF exchange constants along and between the legs, respectively, and the hyperfine parameter ratio $B_\parallel/A_\parallel \sim -0.1$,[37] where $\parallel$ indicates the direction perpendicular to the ladders. Takigawa *et al.* reported the T_{2G} measurement on the linear spin-chain Sr_2CuO_3.[44] They observed the T dependence of $1/T_{2G} \propto 1/\sqrt{T}$ to be consistent with the scaling theory developed by Sachdev.[48] The value of

$$\left(\frac{T_{2G}}{T_1\sqrt{T}}\right)_z=\frac{A_x^2(\pi)+A_y^2(\pi)}{A_z^2(\pi)}\,\frac{4}{I}\sqrt{\frac{\pi}{pJ}}, \qquad (4)$$

was in quantitative agreement with the theoretical prediction for $J_\parallel=2200$ K.[44] Here $I=8.4425$ and $p=0.69$. Note that the

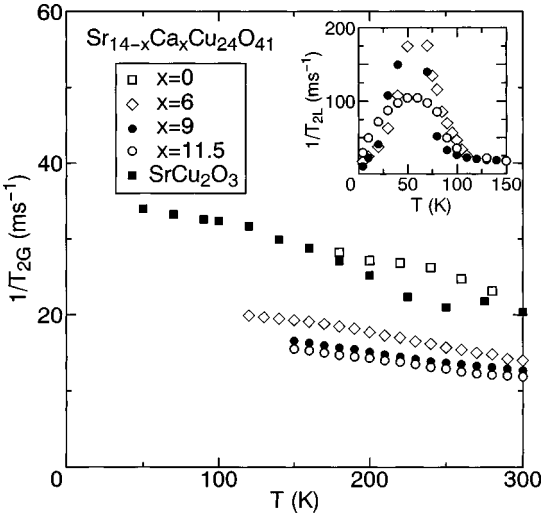

FIG. 13. T dependences of the Gaussian spin-echo decay rate $1/T_{2G}$ at $f=125.1$ MHz in Sr14 (□), Ca6 (◇), Ca9 (●), Ca11.5 (○), and $SrCu_2O_3$ (■) (Ref. 9). The inset indicates the T dependences of the Lorentzian decay rate $1/T_{2L}$ in Ca6 (◇), Ca9 (●), and Ca11.5 (○).

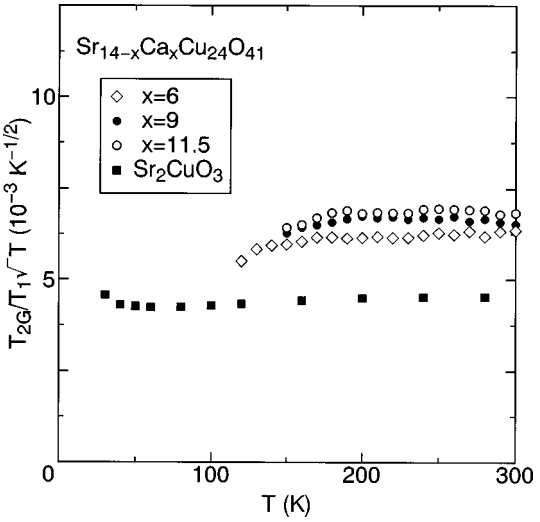

FIG. 14. T dependences of $T_{2G}/T_1\sqrt{T}$ in Ca6 (◇), Ca9 (●), Ca11.5 (○), and Sr_2CuO_3 (■) (Ref. 44).

T dependence of the inverse spin correlation length ξ_{1D}^{-1} of the $S=1/2$ spin-chain is proportional to the temperature $\xi_{1D}^{-1}\propto T$.[49] T_{2G}^2 proportional to the temperature is hence related to ξ_{1D}^{-1} from the relation of $T_{2G}^2\propto T\propto\xi_{1D}^{-1}$. In the two-leg spin-ladder systems with isotropic intra-ladder exchange couplings $J_\parallel=J_\perp$ we found the relation of $T_{2G}^2=\alpha+\beta\xi_{\text{ladder}}^{-1}$. This relation was obtained from a comparison of the T dependence between $1/T_{2G}$ (Ref. 37) and ξ_{ladder} (Ref. 50) calculated by the quantum Monte Carlo method. Note that $\alpha=0$ for $J_\perp=0$. α is negligible in the weak coupling regime with $J_\perp/J_\parallel\leqslant 0.5$ for the two-leg spin-ladder systems, although the calculation of $1/T_{2G}$ is not currently available. In $T\leqslant 0.25\Delta$ where ξ_{ladder} is independent of the temperature, $1/T_{2G}$ was shown to be invariant as well.[37,50]

Figure 13 indicates the T dependence of $1/T_{2G}$ along with the data for $SrCu_2O_3$.[9] Below ~150 K, an increase in the NMR linewidth prevents precise measurements of T_{2G}. The spin-echo decay curve also changes from a Gaussian to a Lorentzian type. Furthermore, $1/T_{2L}$ shows a pronounced peak at $T_L\sim$ 60 K for Ca6 and Ca9 and a broad peak for Ca11.5 as shown in the inset of Fig. 13. This anomaly in $1/T_{2L}$ points to an intimate relation between the transport and the magnetic properties. Since mobile holes begin to localize upon cooling due to a quasi-1D-like conducting channel, the peak in $1/T_{2L}$ is caused when the frequency of spin fluctuations along the magnetic field is comparable to the NMR frequency at $T_L\sim 60$ K and the activation law in $1/T_1$ is masked below T_L. In order to extract a characteristic of spin correlations inherent to the metallic spin-ladder systems with mobile holes, we focus on the data at high T where the spin-echo decay follows the Gaussian type.

$1/T_{2G}$ is suppressed by the increasing Ca content. T_{2G}^2 follows T linear behavior above ~200 K. Accordingly, from the relation of $T_{2G}^2\sim\beta\xi_{\text{ladder}}^{-1}\sim T$, the spin correlation length ξ_{ladder} in Ca6, Ca9, and Ca11.5 decreases upon heating. Together with the relaxation behavior of $1/T_1=$const above 200 K presented in Fig. 12, the spin dynamics of these compounds are consistent with the behavior of the $S=1/2$ 1D Heisenberg systems. As indicated in Fig. 14, $(T_{2G}/T_1\sqrt{T})_b$ for Ca6, Ca9, and Ca11.5 does not depend on the temperature in the range of 180−300 K. Its magnitude is somewhat larger than in Sr_2CuO_3.[44] From Eq. (4), it is seen that $J_\parallel$ is smaller for Ca6, Ca9, and Ca11.5 than $J_\parallel=2200$ K for Sr_2CuO_3. It should be stressed that the scaling of T_{2G}/T_1T for underdoped high-T_c cuprates with a pseudogap is not valid at all as displayed in Fig. 15 where T_{2G}/T_1T for $YBa_2Cu_4O_8$ remains constant above ~150 K.[51]

By inserting the experimental value of $2A_a^2(\pi)/A_b^2(\pi)=2/(2R_{q=\pi}-1)=0.263$ into Eq. (4), $(T_{2G}/T_1\sqrt{T})_b=6.9\times10^{-3}$ K$^{-1/2}$ is in excellent agreement with the calculation using $J_\parallel\sim 1500$ K for Ca11.5. From the same analysis, $J_\parallel$ is estimated as ~1800 and ~1500 K for Ca6 and Ca9, respectively. This is rather close to $J_\parallel=2200$ K for Sr_2CuO_3,[44] but is twofold the exchange constant of $J_\parallel=850$ K for

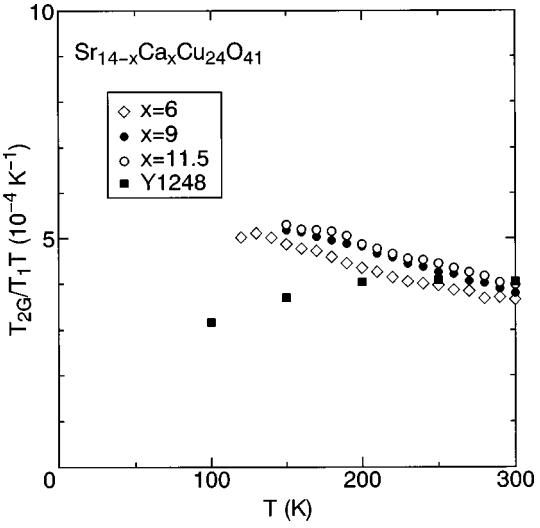

FIG. 15. Comparison with scaling in the underdoped high-T_c cuprate of $YBa_2Cu_4O_8$ (■) (Ref. 51) in which $T_{2G}/T_1T=$const is valid. In Ca6 (◇), Ca9 (●), and Ca11.5 (○), T_{2G}/T_1T depends on the temperature for the ladder systems.

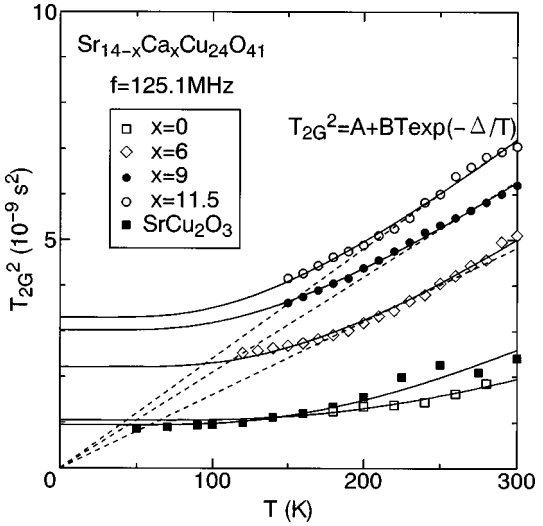

FIG. 16. T dependences of T_{2G}^2 in Sr14 (□), Ca6 (◇), Ca9 (●), Ca11.5 (○), and $SrCu_2O_3$ (■) (Ref. 9). Respective solid line is a fit to $T_{2G}^2 = A + BT\exp(-\Delta/T)$ with $\Delta = 550$, 350, 280, 270, and 400 K for Sr14, Ca6, Ca9, Ca11.5, and $SrCu_2O_3$.

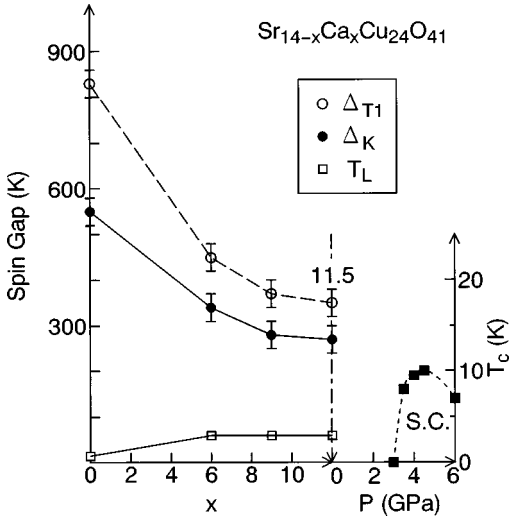

FIG. 17. Phase diagrams of spin gap upon Ca substitution and of superconductivity as a function of pressure. The spin gaps Δ_K (●) and Δ_{T_1} (○) are obtained from the Knight shift and the T_1 measurements, respectively. T_c is also plotted by solid square (scale on the right axis) (Ref. 2). T_L(□) for Sr14 is the temperature at which $1/T_1$ in the ladder Cu sites measured by NMR has a peak, whereas T_L for Ca6, Ca9, and Ca11.5 is defined as the temperature at which $1/T_{2L}$ has a peak associated with a localization of mobile pairs.

$SrCu_2O_3$.[37] From the analysis of $\chi(T)$ in $SrCu_2O_3$, Johnston suggested $J_\perp/J_\parallel \sim 0.5$ with $J_\parallel \sim 2000$ K.[52] For $J_\perp/J_\parallel \leqslant 0.5$, $J_\perp$ is estimated to be ~ 700 K from the relation of $\Delta = 0.41 J_\perp$ (Ref. 50) using $\Delta = 280 \sim 270$ K. Since T_1 and T_{2G} were measured in the T range of $100-300$ K, which is much lower than $J_\perp \sim 700$ K, the situation seems to be far from the condition where each chain is isolated. One may wonder if the spin dynamics should not be described by the 1D-like behavior.

On this point, we remark that the presence of mobile holes in the two-leg spin-ladder system affects the spin correlation in Ca6, Ca9, and Ca11.5. In the undoped two-leg spin-ladder systems, the heuristic form of

$$\xi_{\text{ladder}}^{-1}(T) = \xi_0^{-1} + \xi_{1D}^{-1}(T)\exp(-\Delta/T)$$

described the spin correlation length data using the Monte Carlo calculation.[50] Here, $\xi_0^{-1} = \Delta/c_{1D}$ is the finite value at low T associated with the quantum disordered state with the spin gap. By combining the relation of $T_{2G}^2(T) = \alpha + \beta\xi_{\text{ladder}}^{-1}(T)$ with the above heuristic form, the T dependence of T_{2G}^2 is described by $A + BT\exp(-\Delta/T)$ as shown by the solid line in Fig. 16 where the experimental values of $\Delta = 550$, 350, 280, 270, and 400 K are used for Sr14, Ca6, Ca9, Ca11.5, and $SrCu_2O_3$,[9] respectively.

In the undoped two-leg spin-ladder systems, $T_{2G}^2(T=0) = A_0$ is scaled to $\xi_0^{-1} = \Delta/c_{1D}$. Since the Δ's in Ca6, Ca9, and Ca11.5 are smaller than those in $SrCu_2O_3$ and Sr14, $T_{2G}^2(T=0) = A_h$ for Ca6, Ca9, and Ca11.5 should be smaller than those for the latter since $A_0 \propto \Delta$. This is, however, not the case since $A_h \propto \xi_{\text{eff}}^{-1} \gg A_0 \propto \xi_0^{-1}$ as seen in Fig. 16. The spin correlation length in Ca9 and Ca11.5 is apparently reduced due to the existence of mobile holes in the two-leg spin-ladder systems. A temperature crossover of spin correlations in the 1D Hubbard model close to half filling was studied by Iino and Imada.[53] In a doped compound with a concentration of x, the growth of spin correlations saturates upon cooling at a value determined from $\xi_h \sim d$, where d is the average distance among mobile holes, i.e., $d = 1/x$. This is because an effective spin correlation length ξ_{eff} is described as $\xi_{\text{eff}}^{-1} = \xi_h^{-1} + \xi_0^{-1}$. In applying this relation to doped two-leg spin-ladder systems, we assume that $A_h \sim \xi_{\text{eff}}^{-1} = \xi_h^{-1} + \xi_0^{-1}$ for Ca6, Ca9, and Ca11.5. Our experiment suggests $\xi_h^{-1} \gg \xi_0^{-1}$. This scaling enables us to estimate a possible value of ξ_h and, hence, an effective hole content x. If mobile holes were absent, $\xi_0/a \sim$ 5.2, 7.6, 9.5, and 9.9 for Sr14, Ca6, Ca9, and Ca11.5 would be estimated from $\xi_0 = c_{1D}/\Delta$ with $J_\parallel \sim 1800$ K for Ca6 and $J_\parallel \sim 1500$ K for Ca9 and Ca11.5 and by using $\Delta = 540$ K (Sr14), 350 K (Ca6), 280 K (Ca9), and 270 K (Ca11.5). By scalings such as $A_0(\text{Ca6})/A_0(\text{Sr14}) \sim \xi_0^{-1}(\text{Ca6})/\xi_0^{-1}(\text{Sr14}) \sim 0.64$, $A_0(\text{Ca9})/A(\text{Sr14}) \sim 0.62$, and $A_0(\text{Ca11.5})/A(\text{Sr14}) \sim 0.60$, A_0 would be related to a possible value of $T_{2G}^2(T=0)$ for Ca6, Ca9, and Ca11.5 if the mobile holes were absent. Then, we can estimate from $A_h/A_0 \sim (\xi_h^{-1} + \xi_0^{-1})/\xi_0^{-1}$ the values of $\xi_h(\text{Ca6}) \simeq$ 3.4, $\xi_h(\text{Ca9}) \simeq$ 2.3, and $\xi_h(\text{Ca11.5}) \simeq 2.0$. In addition, from the relation of $x = (2d)^{-1} = (2\xi_h)^{-1}$ an effective hole content x per Cu_2O_3 ladder is suggested from the relation of $x = (2d)^{-1} = (2\xi_h)^{-1}$ to be $\sim$0.14, 0.22, and 0.25 for Ca6, Ca9, and Ca11.5, respectively. Interestingly, these values of effective hole content are compatible with $x \sim 0.14$, 0.2, and 0.22 estimated from the optical conductivity measurement of Ca6, Ca9, and Ca11, respectively, as reported by Osafune *et al.*[24]

The spin gap and 1D-like spin dynamics in $Sr_{14-x}Ca_xCu_{24}O_{41}$ are almost unchanged regardless of the increase in the doping level. The conductivity increases and the spin correlation length decreases with the increasing Ca content. Thus, Ca6, Ca9, and Ca11.5 are doped two-leg spin-ladder compounds with the spin gap and 1D-like spin dynamics.

IV. CONCLUSION

Comprehensive NMR studies have clarified the spin gap states and the spin dynamics in the single crystals of $Sr_{14-x}Ca_xCu_{24}O_{41}$. The results obtained are summarized in Fig. 17.

(1) The spin gaps obtained from the measurements of the Knight shift and T_1, Δ_K and Δ_{T_1}, decrease significantly as the Ca substitution increases. Although this trend was reported from the T_1 measurements on the polycrystal samples up to Ca9,[17] it should be noted that the magnitudes of $\Delta_{T_1,\mathrm{poly}}$ are not consistent with those of the present $\Delta_{T_1,\mathrm{single}}$. This is because T_1 in the polycrystal samples is not uniquely determined in contrast to the case of the single crystals.

(2) The spin gap persists with $\Delta_K=270$ K and $\Delta_{T_1}=350$ K up to Ca11.5, in which superconductivity was discovered by applying pressure higher than 3.5 GPa, as indicated in Fig. 17.[2] The magnitude of the spin gap and the 1D-like aspect of spin dynamics are almost *unchanged* by an increase in the hole doping level. In contrast, the conductivity increases markedly with increasing hole density.

(3) Systematic T_{2G} measurements probing the spin correlation length ξ demonstrate that holes are doped with a content of $x\sim 0.14$, 0.22, and 0.25 per Cu_2O_3 ladder for Ca6, Ca9, and Ca11.5, respectively.

(4) The staggered spin fluctuations around $q\sim\pi$ dominate the nuclear relaxation process below $T_L\sim 60$ K for Ca6, Ca9, and Ca11.5. This low-T anomaly in spin dynamics is caused by the localization effect of mobile holes as evidenced by the increased resistivity below T_L.[2,45]

Further insights are extracted from a comparison between the magnetic and the transport properties shown in Fig. 18. In the high-T region bounded by the dash-dotted line, the spin dynamics are consistent with the scaling theory for the $S=1/2$ 1D Heisenberg model. In this regime, the resistivity along the c axis (the leg) exhibits metallic behavior with linear T dependence, whereas that along the a axis perpendicular to the c axis is weakly dependent of the temperature with an order of magnitude larger resistivity than that along the c axis.

In the low-T region where the spin gap opens, the behavior of the resistivity parallel to the c axis deviates slightly from the linear T behavior, but that perpendicular to the c axis begins to *increase*. In this regime, pairs are formed accompanying the spin gap, but confined in each ladder. Therefore, anisotropic transport is enhanced. An appearance of bound pairs was also suggested from an analyses of the transport data.[45]

Upon cooling below T_L, marked by the dashed line, bound pairs start to be localized by the randomness in the quasi-1D conducting channel along the c axis. As a result, the metallic state with the spin gap changes to localized states of bound pairs in which the resistivity increases following the T^{-2} power law below $T_L\sim 60$ K.

Notably, $Sr_{2.5}Ca_{11.5}Cu_{24}O_{41}$ is the first hole-doped two-leg spin-ladder compound in which pressure-induced superconductivity has been discovered.[1,2] It has been found that its metallic state is dominated by the 1D-like spin dynamics at high T and accompanied by the spin gap formation at low T.

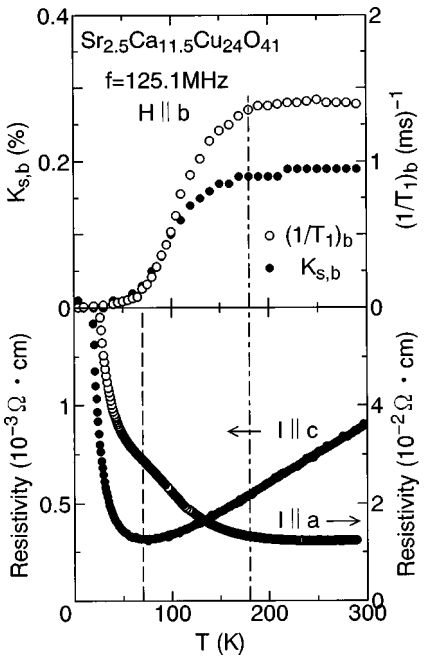

FIG. 18. A comparison between the magnetic and the transport properties in Ca11.5. The upper panel indicates the T dependences of the spin part in the Knight shift $K_{s,b}(T)$ and $(1/T_1)_b$ for the $H\|b$ axis. The lower panel is the T dependences of the resistivity along the c axis (scale on the left axis) and the a axis (scale on the right axis). In a T range higher than the temperature marked by the dashed-dot line, the spin dynamics in the ladder Cu sites is characterized by the 1D-like behavior and the resistivity exhibits the T linear behavior. T_L is indicated by dashed line. In T range down to T_L, pairs are formed with the spin gap and the metallic state behaves as quasi-1D, exhibiting an anisotropic T dependence of the resistivity. This increasing anisotropy in resistivity is due to the confinement of bound pairs in each ladder. Below T_L, the T dependence of resistivity exhibits an upturn due to the localization of mobile pairs. Correspondingly, staggered spin fluctuations are induced in the ladders, dominating the nuclear relaxation process at the low-temperature regime.

Preformed pairs are confined in each ladder below $\sim$180 K and localized below $\sim$60 K at an ambient pressure. An underlying issue is whether or not the application of pressure makes preformed pairs conductive along the ladder and coherently hop in the direction perpendicular to the ladder and, as a result, superconduct. In order to unravel this novel superconducting mechanism, a further key experiment must be conducted using NMR under high pressure, and is in progress.

ACKNOWLEDGMENTS

The authors would like to express thanks to T. M. Rice, H. Fukuyama, M. Imada, N. Nagaosa, M. Ogata, H. Tsunetsugu, M. Takano, S. Uchida, B. Battlog, Y. Koike, and H. Eisaki for stimulating discussions and comments. This work has been supported by CREST (Core Research for Evolutional Science and Technology) of Japan Science and Technology Corporation (JST) and also partly by a Grant-in-Aid from the Ministry of Education, Science and Culture of Japan.

[1] M. Uehara, T. Nagata, J. Akimitsu, H. Takahashi, N. Môri, and K. Kinoshita, J. Phys. Soc. Jpn. **65**, 2764 (1996).
[2] T. Nagata, M. Uehara, J. Goto, N. Komiya, J. Akimitsu, N. Motoyama, H. Eisaki, S. Uchida, H. Takahashi, T. Nakanishi, and N. Môri, Physica C **282-287**, 153 (1997).
[3] E. Dagoto and T. M. Rice, Science **271**, 618 (1996).
[4] E. Dagoto, J. Riera, and D. J. Scalapino, Phys. Rev. B **45**, 5744 (1992).
[5] T. M. Rice, S. Gopalan, and M. Sigrist, Europhys. Lett. **23**, 445 (1993); M. Sigrist, T. M. Rice, and F. C. Zhang, Phys. Rev. B **49**, 12 058 (1994).
[6] D. C. Johnston, J. W. Johnson, D. P. Goshorn, and A. J. Jacobson, Phys. Rev. B **35**, 219 (1987).
[7] R. S. Eccleston, T. Barnes, J. Brody, and J. W. Johnson, Phys. Rev. Lett. **73**, 2626 (1994).
[8] M. Azuma, Z. Hiroi, M. Takano, K. Ishida, and Y. Kitaoka, Phys. Rev. Lett. **73**, 3463 (1994).
[9] K. Ishida, Y. Kitaoka, K. Asayama, M. Azuma, Z. Hiroi, and M. Takano, J. Phys. Soc. Jpn. **63**, 3222 (1994); K. Ishida, Y. Kitaoka, Y. Tokunaga, S. Matsumoto, K. Asayama, M. Azuma, Z. Hiroi, and M. Takano, Phys. Rev. B **53**, 2827 (1996).
[10] E. M. MaCarron, M. A. Subramanian, J. C. Calabrese, and R. L. Harlow, Mater. Res. Bull. **23**, 1355 (1988).
[11] T. Siegrist, L. F. Schneemeyer, S. A. Sunshine, J. V. Waszczak, and R. S. Roth, Mater. Res. Bull. **23**, 1429 (1988).
[12] M. Kato, K. Shiota, and Y. Koike, Physica C **255**, 284 (1995).
[13] M. Uehara, M. Ogawa, and J. Akimitsu, Physica C **255**, 193 (1995).
[14] M. Matsuda and K. Katsumata, Phys. Rev. B **53**, 12 201 (1996).
[15] S. A. Carter, B. Batlogg, R. J. Cava, J. J. Krajewski, W. F. Peck, Jr., and T. M. Rice, Phys. Rev. Lett. **77**, 1378 (1996).
[16] J. Akimitsu, M. Uehara, T. Nagata, S. Matsumoto, Y. Kitaoka, H. Takahashi, and N. Môri, Physica C **263**, 475 (1996).
[17] S. Tsuji, K. Kumagai, M. Kato, and Y. Koike, J. Phys. Soc. Jpn. **65**, 3474 (1996).
[18] R. S. Eccleston, M. Azuma, and M. Takano, Phys. Rev. B **53**, R14 721 (1996).
[19] M. Matsuda, K. Katsumata, H. Eisaki, N. Motoyama, S. Uchida, S. M. Shapiro, and G. Shirane, Phys. Rev. B **54**, 12 199 (1996).
[20] S. Matsumoto *et al.* (unpublished).
[21] M. Takigawa, N. Motoyama, H. Eisaki, and S. Uchida, Phys. Rev. B **57**, 1124 (1998).
[22] D. Cox *et al.* (unpublished).
[23] K. Magishi, S. Matsumoto, K. Ishida, Y. Kitaoka, K. Asayama, M. Uehara, T. Nagata, and J. Akimitsu, Physica C **282-287**, 1115 (1997).
[24] T. Osafune, N. Motoyama, H. Eisaki, and S. Uchida, Phys. Rev. Lett. **78**, 1980 (1997).
[25] T. Takahashi, T. Yokoya, A. Ashihara, O. Akaki, H. Fujisawa, A. Chainami, M. Uehara, T. Nagata, J. Akimitsu, and H. Tsunetsugu, Phys. Rev. B **56**, 7870 (1997); J. Phys. Chem. Solids (to be published).
[26] Y. Mizuno, T. Tohyama, and S. Maekawa, J. Phys. Soc. Jpn. **66**, 937 (1997).
[27] Y. Kitaoka, K. Magishi, S. Matsumoto, K. Ishida, S. Ohsugi, K. Asayama, M. Uehara, T. Nagata, and J. Akimitsu, J. Magn. Magn. Mater. (to be published).
[28] A. Narath, Phys. Rev. B **13**, 3724 (1976).
[29] C. H. Pennington, D. J. Durand, C. P. Slichter, J. P. Rice, E. D. Bukowski, and D. M. Ginsberg, Phys. Rev. B **39**, 274 (1989); C. H. Pennington and C. P. Slichter, Phys. Rev. Lett. **66**, 381 (1991).
[30] R. E. Walstedt and S-W. Cheong, Phys. Rev. B **51**, 3163 (1995).
[31] M. Troyer, H. Tsunetsugu, and D. Würtz, Phys. Rev. B **50**, 13 515 (1994).
[32] L. van Hove, Phys. Rev. **95**, 1374 (1954).
[33] M. Takigawa, T. Asano, Y. Ajiro, M. Mekata, and Y. J. Uemura, Phys. Rev. Lett. **76**, 2173 (1996).
[34] T. Shimizu, D. E. MacLaughlin, P. C. Hammel, J. D. Thompson, and S-W. Cheong, Phys. Rev. B **52**, R9835 (1995).
[35] H. Iwase, M. Isobe, Y. Ueda, and H. Yasuoka, J. Phys. Soc. Jpn. **65**, 2397 (1996).
[36] Y. Furukawa, A. Iwai, K. Kumagai, and A. Yakubovsky, J. Phys. Soc. Jpn. **65**, 2393 (1996).
[37] A. W. Sandvik, E. Dagotto, and D. J. Scalapino, Phys. Rev. B **53**, R2934 (1996).
[38] J. Kishine and H. Fukuyama, J. Phys. Soc. Jpn. **66**, 26 (1997).
[39] S. Sachdev and K. Damle, Phys. Rev. Lett. **78**, 943 (1997).
[40] A. Abragam, *The Principles of Nuclear Magnetism* (Clarendon, Oxford, 1961).
[41] M. Takigawa, P. C. Hammel, R. H. Heffner, Z. Fisk, J. L. Smith, and R. B. Schwarz, Phys. Rev. B **39**, 300 (1989).
[42] F. Mila and T. M. Rice, Physica C **157**, 561 (1989); Phys. Rev. B **40**, 11 382 (1989).
[43] H. Monien, D. Pines, and M. Takigawa, Phys. Rev. B **43**, 258 (1991).
[44] M. Takigawa, N. Motoyama, H. Eisaki, and S. Uchida, Phys. Rev. Lett. **76**, 4612 (1996).
[45] N. Motoyama, T. Osafune, T. Kakeshita, H. Eisaki, and S. Uchida, Phys. Rev. B **55**, R3386 (1997).
[46] D. Thelen and D. Pines, Phys. Rev. B **49**, 3528 (1994).
[47] M. Takigawa, Phys. Rev. B **49**, 4158 (1994).
[48] S. Sachdev, Phys. Rev. B **50**, 13 006 (1994).
[49] K. Nomura and M. Yamada, Phys. Rev. B **43**, 8217 (1991).
[50] M. Greven, R. J. Birgeneau, and U.-J. Wiese, Phys. Rev. Lett. **77**, 1865 (1996).
[51] R. L. Corey, N. J. Curro, K. O'Hara, T. Imai, C. P. Slichter, K. Yoshimura, M. Katoh, and K. Kosuge, Phys. Rev. B **53**, 5907 (1996); N. J. Curro, T. Imai, C. P. Slichter, and B. Dabrowski, *ibid.* **56**, 877 (1997).
[52] D. C. Johnston, Phys. Rev. B **54**, 13 009 (1996).
[53] Y. Iino and M. Imada, J. Phys. Soc. Jpn. **64**, 4392 (1995).